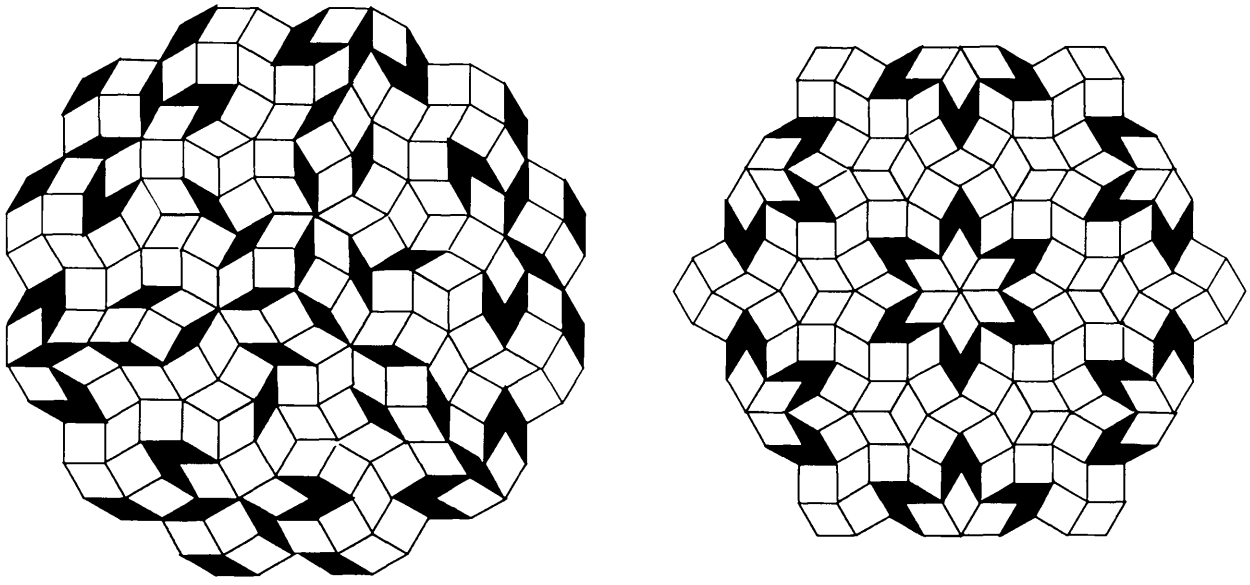

(*a*) (*b*)

Fig. 10. (*a*) 3-fold rotational symmetry, 2nd generation. (*b*) 6-fold rotational symmetry, 2nd generation.

projections and indentations of Fig. 8(*c*) make it look like a possible violation, but in fact it is simply a generalized square, *i.e.* a new aspect of the solution. The reader will see how the projections and indentations work in Fig. 10.

As first-generation models for tilings with 3- and 6-fold rotational symmetry we use the configurations of Figs. 9(*b*) and (*d*), respectively. We go to the next generation, Fig. 10, by replacing the prototiles of Fig. 9 with the tiles of Fig. 8. We could do the same in Figs. 9(*a*), (*c*), (*e*).

The proofs of the validity (*i.e.* absence of interior edge violations) of the tilings of the infinite plane obtained by substituting higher-generation tiles into the configurations of Fig. 9 and passing to the limit, as well as the uncountable infinity of these tilings, follow the line of arguments given in §1.

References

BRUIJN, N. G. DE (1981). *Proc. K. Ned. Akad. Wet. Ser. A*, **43**, 39-66.

CLARK, D. S. & SURYANARAYAN, E. R. (1991). Submitted to *J. Comb. Theor. Ser. B.*

GRÜNBAUM, B. & SHEPHARD, G. C. (1987). *Tilings and Patterns.* New York: W. H. Freeman.

WATANABE, Y., ITO, M. & SOMA, T. (1987). *Acta Cryst.* A**43**, 133-134.

WHITTAKER, E. J. W. & WHITTAKER, R. M. (1988). *Acta Cryst.* A**44**, 105-112.

Acta Cryst. (1991). A**47**, 502-510

Polarization Effects on X-ray Multiple Diffraction

BY SHAW-WEN LUH AND SHIH-LIN CHANG

Department of Physics, National Tsing Hua University, Hsinchu, Taiwan

(*Received* 29 *August* 1990; *accepted* 18 *March* 1991)

Abstract

The effects of polarization on X-ray multiple diffraction are investigated experimentally. Polarized and unpolarized incident beams are used in multiple diffraction experiments for GaAs and Ge crystals. All the three-beam diffractions in a 360° azimuthal rotation of the crystals are analyzed for diffracted intensities and phase determination, based on the article by Chang & Tang [*Acta Cryst.* (1988), A**44**,

0108-7673/91/050502-09$03.00

1065–1072]. Comparison with other proposed models is also given. It is found that the peak intensities of most reflections decrease and the widths at half-maxima increase for the polarized-beam experiments, compared with the unpolarized ones. Moreover, some of the diffraction peaks disappear due to polarization. The values of the triplet phase determined from three-beam diffraction intensities agree well with the theoretical ones, provided that the polarization factors have been taken into account in the analysis procedure.

I. Introduction

X-ray multiple diffraction takes place when a single crystal is so oriented that two or more sets of atomic planes simultaneously satisfy Bragg's law for a given X-ray wavelength (Renninger, 1937). Interference among multiply diffracted waves has been demonstrated to be the mechanism which conveys the phase information of the involved structure-factor multiplets *via* the intensity variation of the diffracted beams (Post, 1977; Chapman, Yoder & Colella, 1981; Høier & Aanestad, 1981; Chang, 1982; Hümmer & Billy, 1982; Juretschke, 1982*a*). Applications of this diffraction technique for phase determination in real crystals have recently been reported (Shen & Colella, 1988; Mo, Hauback & Thorkildsen, 1988; Hümmer, Weckert & Bondza, 1989; Chang, Huang, Tang & Lee, 1989).

Polarization, which is always considered as an important factor affecting intensity measurements, has long been known to complicate the phase-determination procedures in multiple diffraction experiments (Lipscomb, 1949). In a two-beam approximation for three-beam diffraction, Juretschke (1982*b*, 1986) demonstrated analytically how σ- and π-polarized waves affect the diffraction intensities of the exact three-beam diffraction positions. In this paper, we report the experimental results of multiple diffraction with unpolarized and σ-polarized incident beams. The intensity variations of the multiply diffracted beams due to different polarizations are observed and interpreted in terms of the kinematical theory (Moon & Shull, 1964; Caticha-Ellis, 1969; Prager, 1971) and dynamical approaches (Juretschke, 1982*a*, *b*, 1986; Chang & Tang, 1988). The determination of phases on a quantitative basis is also attempted for the experiment with the σ-polarized incident beam.

II. Theoretical considerations

We briefly outline here the kinematical and dynamical approaches concerning the polarization effects on multiple diffraction intensities. The formalism given below will be used to analyze the experimentally obtained intensities.

(i) *Kinematical theory*

The power-transfer equations are usually employed to account for diffraction intensities in multiple diffraction experiments (Moon & Shull, 1964; Zachariasen, 1965; Caticha-Ellis, 1969; Prager, 1971). The expression for the diffraction intensity of a given G reflection in a three-beam $(0, G, L)$ diffraction takes the form

$$R_p(G) \propto -p_{GL}(M)K_{GL}(M)Q_L - p_{GM}(L)K_{GM}(L)Q_M + p_{LM}(G)K_{LM}(G)Q_LQ_M/Q_G \quad (1)$$

where 0 is the incident diffraction, G and L are the primary and secondary reflections, respectively. $M = G - L$ is the coupling between G and L reflections. Q_G and $K_{LM}(G)$ are the effective reflectivity and Lorentz factor defined as

$$Q_G = \lambda^3 N_0^2 |F_G|^2/\sin 2\theta_G \quad (2)$$

$$K_{LM}(G) = \sin 2\theta_G/(\sin\psi \cos\chi \cos\zeta), \quad (3)$$

where θ_G and F_G are the Bragg angle and structure factor of the G reflection. N_0 is the number of unit cells per volume. χ and ζ are the angles between the equatorial plane of the Ewald sphere and the diffracted L and M beams, respectively (Prager, 1971). ψ is the angle between the L and M diffracted beams projected onto the equatorial plane. λ is the X-ray wavelength used. The polarization factors $p_{ij}(m)$ are derived from the consideration that a three-beam diffraction is treated as a combination of successive reflections. The $p_{ij}(m)$ in (1) is then defined as (Zachariasen, 1965)

$$p_{ij}(m) = \tfrac{1}{2}[\cos^2 2\theta_i + \cos^2 2\theta_j + (\cos 2\theta_m - \cos 2\theta_i \cos 2\theta_j)^2]/p_2 \quad (4)$$

without a monochromator and as (Caticha-Ellis, 1969)

$$p_{ij}(m) = \tfrac{1}{2}\{[1 - (\cos 2\theta_m - \cos 2\theta_i \cos 2\theta_j)^2/\sin^2 2\theta_i] \times \cos^2 2\theta_i(1 - \sin^2 2\alpha \cos^2\gamma) + [(\cos 2\theta_m - \cos 2\theta_i \cos 2\theta_j)^2/\sin^2 2\theta_i + \cos^2 2\theta_j](\sin^2 2\alpha \cos^2\gamma + \cos^2 2\alpha)\}/p_2 \quad (5)$$

with a monochromator in front of the crystal sample. m is the coupling between i and j. p_2 is the two-beam polarization factor of the G reflection, *i.e.*

$$p_2 = \tfrac{1}{2}(1 + \cos^2 2\theta_G). \quad (6)$$

γ is the angle between the planes of incidence of the monochromator and the ith reflection. α is the Bragg angle of the reflection used to monochromatize the incident beam. Equation (5) reduces to (4) as $\alpha = 0$.

(ii) *Two-beam dynamical approximation for the three-beam case near the three-beam point*

Juretschke (1982*a*, *b*) has considered the dynamical nature of a three-beam (0, *G*, *L*) diffraction near the exact three-beam diffraction position and derived the following expressions for the intensity ratio of three-beam and two-beam (the *G*-reflection) diffractions:

$$I_3/I_2=[1+(2/\chi)\cos\delta_3+1/\chi^2]^n, \tag{7}$$

where n is equal to 1/2 for a strong G reflection and 1 for a weak reflection. δ_3 is the phase of the structure-factor triplet $F_L F_{G-L}/F_G$. The term $1/\chi$ is defined as

$$1/\chi=\Gamma\pi_1(F_L F_{\bar{L}-\bar{G}}/F_G)\times[(2\cos\theta_G\cos\theta_l\sin\varphi_l)/\tan\Delta\varphi]^{-1} \tag{8}$$

for σ-polarized waves and

$$1/\chi=\Gamma\pi_6(F_L F_{\bar{L}-\bar{G}}/F_G)\times[(2\cos\theta_G\cos\theta_l\sin\varphi_l)/\tan\Delta\varphi]^{-1} \tag{9}$$

for π-polarized waves. π_1 and π_6 are defined as (Juretschke 1986)

$$\pi_1=\cos^2\varphi_l+\sin^2\varphi_l\sin^2\theta_l \tag{10}$$

$$\pi_6=\cos^2\theta_G\cos^2\theta_l-\sin^2\theta_G\times(\sin^2\varphi_l+\cos^2\varphi_l\sin^2\theta_l), \tag{11}$$

where $\Delta\varphi$ is the azimuthal angle of rotation around the reciprocal-lattice vector $\mathbf{g}$ of the G reflection. φ_l is the angle between the wavevector $\mathbf{K}_L$ of the L reflection and the plane of incidence of the G reflection. $\pi/2-\theta_l$ is the angle between $\mathbf{K}_L$ and $\mathbf{g}$. The direction of $\mathbf{K}_L$ is that of the L-reflected beam. Γ is a constant equal to $-e^2\lambda^2/mc^2\pi V$ where e and m are the charge and mass of an electron, respectively. V is the volume of the unit cell.

The factors π_1 and π_6 can be considered as the σ- and π-polarization factors of the three-beam diffraction. They can be rearranged, in terms of the Bragg angles θ_G, θ_L and θ_{G-L} of the G, L and $G-L$ reflections, as

$$\pi_1=[\cos^2 2\theta_{G-L}+\cos^2 2\theta_L+2\cos 2\theta_G\cos^2 2\theta_L\cos^2 2\theta_{G-L}]/\sin^2 2\theta_G \tag{12}$$

$$\pi_6=\cos 2\theta_G-[(\cos 2\theta_{G-L}-\cos 2\theta_G\cos 2\theta_L)^2+(\cos 2\theta_L-\cos 2\theta_G\cos 2\theta_{G-L})^2]/2\sin^2 2\theta_G. \tag{13}$$

The corresponding $1/\chi$ becomes

$$1/\chi=\pi_1\Gamma P_0(F_L F_{\bar{L}-\bar{G}}/2F_G)/\tan\Delta\varphi \tag{14}$$

for σ polarization and

$$1/\chi=\pi_6\Gamma P_0(F_L F_{\bar{L}-\bar{G}}/2F_G)/\tan\Delta\varphi \tag{15}$$

for π polarization, where

$$P_0=\tfrac{1}{2}[\sin^2 2\theta_G-\cos^2 2\theta_{G-L}-\cos^2 2\theta_L+2\cos 2\theta_G\cos 2\theta_{G-L}\cos 2\theta_L]. \tag{16}$$

This two-beam approximation is valid for the reciprocal-lattice point of the secondary L reflection being far enough from the surface of the Ewald sphere such that the corresponding resonance error satisfies the condition

$$\xi_L\gg(k\Gamma/2)|F_L||F_{\bar{L}-\bar{G}}|/|F_G| \tag{17}$$

where

$$\xi_L=(\mathbf{K}_L\,.\,\mathbf{K}_L)^{1/2}-k(1-\chi_0/2). \tag{18}$$

$\chi_0/4\pi=\Gamma F_0/4\pi$ is the electric susceptibility of the direct diffraction. Clearly, this approach cannot be used to describe the X-ray wavefields inside the crystal at the exact three-beam diffraction position.

(iii) *Modified two-beam dynamical approximation and quantitative phase analysis*

In order to describe the diffraction intensities at the exact three-beam point, Chang & Tang (1988) introduced an imaginary part to the denominator of the resonance function and derived from the fundamental equation of the wavefield the following expression for the G-reflected intensity in a three-beam (0, *G*, *L*) case:

$$I'_G=[I_G(3)-I_G(2)]/I_G(2)=I_D+I_K, \tag{19}$$

where the dynamical intensity I_D and kinematical intensity I_K are defined as (Chang, Huang, Tang & Lee, 1989)

$$I_D=2Pa_1Q[2(\Delta\varphi)\cos\delta_3-\eta_T\sin\delta_3] \tag{20}$$

$$I_K=a_2\eta_T P^2/\eta_i, \tag{21}$$

in which

$$P=|\Gamma|kL_F Q(|F_{G-L}||F_L|/|F_G|) \tag{22a}$$

$$Q=1/[(\Delta\varphi)^2+(\eta_T/2)^2]^{1/2} \tag{22b}$$

$$W=kl\sin\alpha_0\sin\beta_0\cos\theta_G \tag{22c}$$

$$L_F=k/W \tag{22d}$$

$$\eta_T=\eta_i+\eta_B+\eta_M \tag{22e}$$

$$\eta_i=k^2|\chi_0|/W. \tag{22f}$$

Note that here P and Q are redefined to give a compact form for I_K. They are different from those originally given by Chang & Tang (1988). a_1 and a_2 are the polarization factors defined as

$$a_1=\tfrac{1}{2}(B_0+B_5\cos 2\theta_G)/p_2 \tag{23}$$

$$a_2=\tfrac{1}{2}(B_0^2+B_3^2+B_4^2+B_5^2)/p_2, \tag{24}$$

where

$$B_0=1-(l/K)^2\sin^2\alpha_0\sin^2\beta_0 \tag{25a}$$

$$B_3=3(l/K)\sin\alpha_0\sin\beta_0[(l/K)\sin\alpha_0\cos\beta_0\sin\theta_G+(l/K)\cos\alpha_0\cos\theta_G-2\sin 2\theta_G] \tag{25b}$$

$$B_4 = (l/K)^2(\cos\alpha_0\cos\theta_G - \sin\alpha_0\cos\beta_0\sin\theta_G) \times \sin\alpha_0\sin\beta_0 \quad (25c)$$

$$B_5 = \cos 2\theta_G - B_3B_4/[(l/K)\sin\alpha_0\sin\beta_0]^2. \quad (25d)$$

η_T is the total experimental width at half-maximum of the three-beam intensity profile. η_i, η_B and η_M are the intrinsic width, the average instrumental broadening and crystal mosaic spread, respectively. $\Delta\varphi$ is the angular deviation from the exact three-beam position. $k = 1/\lambda$ and **l** is the reciprocal-lattice vector of the L reflection. k/W is the Lorentz factor L_F which is proportional to $K_{LM}(G)$ of (3). α_0 is the angle between the vectors **g** and **l** and β_0 is the angle between $\mathbf{l}_\perp$ and the plane of incidence of the G reflection, $\mathbf{l}_\perp$ being the component of **l** normal to **g**. The factor a_2 of (24) can be expressed in terms of θ_G, θ_L and θ_{G-L} as

$$a_2 = \tfrac{1}{2}[\cos^2 2\theta_{G-L} + \cos^2 2\theta_L + (\cos 2\theta_G - \cos 2\theta_{G-L}\cos 2\theta_L)^2]/p_2. \quad (26)$$

This is exactly the same as $p_{ij}(m)$ given in (4) for $i = G - L$, $j = L$ and $m = G$.

It should be noted that I_K in (21) is suited to *Umweganregung* cases (Renninger, 1937) where the primary G reflection is weak. For an *Aufhellung* case (Renninger, 1937) with a strong G reflection, I_K takes the following form (Chang, Huang, Tang & Lee, 1989):

$$I_K = (\eta_T/\eta_i)k^2\Gamma^2L_F^2Q^2R \quad (27)$$

with

$$R = [a_2|F_{G-L}|^2|F_L|^2 - a_3|F_G|^2|F_L|^2 - a_4|F_G|^2|F_{G-L}|^2]/|F_G|^2, \quad (28)$$

where a_3 and a_4 have the same form as a_2 given in (26) except that the subscripts of the 2θ's have to be permuted according to the subsequent structure factors. Equation (27) is consistent with (1).

To match the theoretical I_K of (21) and the experimental $I_{K,E}$, a scaling constant C_0 is introduced:

$$I_{K,E} = C_0I_K(1/|\gamma_0/\gamma_L|) \quad (29)$$

for a plate-like crystal. The factor γ_0/γ_L is the asymmetry parameter of the secondary L-reflected beam. γ_0 and γ_G are the direction cosines of the incident beam 0 and reflected beam L with respect to the inward crystal-surface normal. [In the previous paper (Tang & Chang, 1988), this weighing factor γ_0/γ_L was employed implicitly so that the formalism given here for I'_G is identical to that derived previously.]

The scaling factor C_0 is determined by comparing the measured $I_{K,E}$ and that calculated at the $\Delta\varphi = 0$ position for all the three-beam cases. With the determined C_0 and the measured peak width η_T, the Lorentzian distribution of I_K can be constructed according to (21) and (29). Subtracting this constructed I_K from the measured profile I'_G, we obtain the phase-dependent dynamical intensity I_D. The triplet phase δ_3 can then be determined according to the relations

$$\cos\delta_3 - \sin\delta_3 = I_+/(2Pa_1QW)|_{\Delta\varphi=\eta_T/2} \quad (30a)$$

$$-\cos\delta_3 - \sin\delta_3 = I_-/(2Pa_1QW)|_{\Delta\varphi=-\eta_T/2} \quad (30b)$$

where

$$I_\pm = I_D(\Delta\varphi = \pm\eta_{T/2}). \quad (31)$$

The sign of the Lorentz factor L_F should also be considered for phase determination (Chang, Huang, Tang & Lee, 1989).

III. Experimental

The experimental set-up with an unpolarized source is the same as that reported previously (Tang & Chang, 1988). Cu $K\alpha_1$ radiation was used. The beam divergence was 0·033° in both vertical and horizontal directions.

The arrangement for the σ-polarized beam is schematically shown in Fig. 1. The set-up consists of (1) an X-ray source from an Elliott GX-21 rotating-anode generator; (2) a 40 cm long collimator with a pinhole of 480 μm diameter at the exit end; (3) a Ge 333 symmetrically cut monochromator used as a polarizer and (4) a four-circle semiautomatic diffractometer (Huber 400). A Cu target and a filament of size 0·5 × 1 mm were used. The beam divergence is 0·03° in the horizontal direction and 0·1° in the vertical direction. The distances between the source, monochromator, crystal sample and detector are also indicated in the same figure.

The crystal sample was first aligned for a given primary reflection G and was rotated around the reciprocal-lattice vector **g** to bring additional sets of atomic planes to satisfy simultaneously Bragg's law. A scintillation counter was used to monitor the G-reflected beam during the azimuthal φ rotation around **g**. The intensity variation on the two-beam

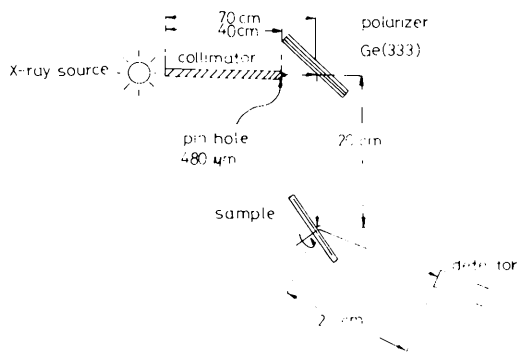

Fig. 1. Schematic representation of the set-up for the σ-polarized beam experiments.

G-reflection background was plotted *versus* φ. Figs. 2, 3 and 4 are such diffraction patterns for Ge 111, 222 and GaAs 222 or Cu $K\alpha_1$, respectively. A slow step scan with 0·01° per step was performed for each three-beam diffraction peak for detailed analysis of intensity and peak width. All the three-beam profiles over 360° azimuth were analyzed. The counting time was chosen so that the statistical error was less than 1%.

IV. Results

Because the vertical divergence of the σ-polarized incident beam is three times wider than that of the unpolarized beam, the peak width of a given multiple diffraction is also three times larger for the σ-polarized beam than that for the unpolarized beam. In addition, owing to the presence of a monochromator, the diffracted intensity with the σ-polarized beam is weaker than that with the unpolarized beam. Keeping these differences in mind, we discuss the polarization effects on the diffraction patterns, peak intensities and peak widths for the following cases.

(i) *Germanium* 111 *multiple diffractions*

111 is a very strong reflection. All the multiple diffractions appear as the *Aufhellung*-type 'dips' in Figs. 2(a) and (b) for the unpolarized and σ-polarized incident beams. Because of the relatively strong intensity of the unpolarized incident beam, the diffraction pattern shows clearly in Fig. 2(a) the intensity asymmetry for the three-beam $202/\bar{1}1\bar{1}$, $\bar{1}1\bar{1}/202$ and $2\bar{2}\bar{4}/\bar{1}35$ reflections and the four-beam $2\bar{2}0$, $\bar{2}20/\bar{1}31$, $3\bar{1}1$ and 311, $\bar{3}11/\bar{1}11$, 400 cases. The indices before and after the slashes indicate the secondary L and the coupling $G-L$ reflections, respectively. The profile asymmetry is not clearly observable in Fig. 2(b) for the σ-polarized beam, except for the $202/\bar{1}1\bar{1}$ case. This is expected because of the large beam divergence and weak intensity of the σ-polarized beam.

The measured relative peak intensities, $(I_2-I_3)/I_2$, the peak widths η_T, the ratios of integrated intensity over $\Delta\varphi$ for the unpolarized and σ-polarized beam experiments, the calculated polarization factors such as a_2's [denoted as $B(\sigma+\pi)$ and $B(\sigma)$] from Chang & Tang (1988), π's from Juretschke (1986) and P's

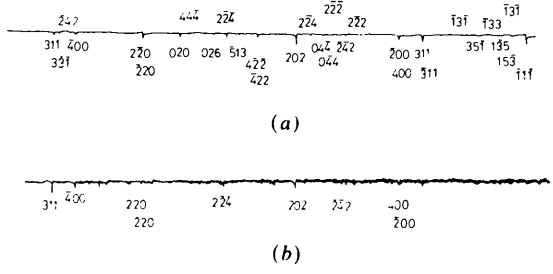

Fig. 2. Multiple diffraction patterns of Ge 111 Cu $K\alpha_1$ for (a) the unpolarized and (b) the σ-polarized beams. The 111 background is at 55% for (a) and 25% for (b) of the full scale 2×10^4 counts s^{-1}.

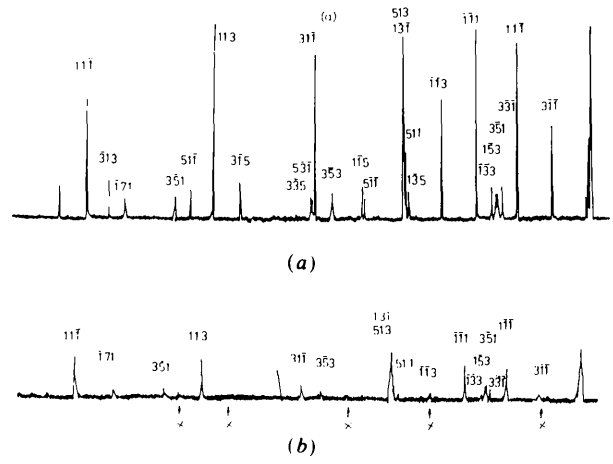

Fig. 3. (a) Multiple diffraction patterns of Ge 222 Cu $K\alpha_1$ for (a) the unpolarized and (b) the σ-polarized beams. The 222 background is at 6% for (a) and 3% for (b) of the full scale of 10^4 counts s^{-1}.

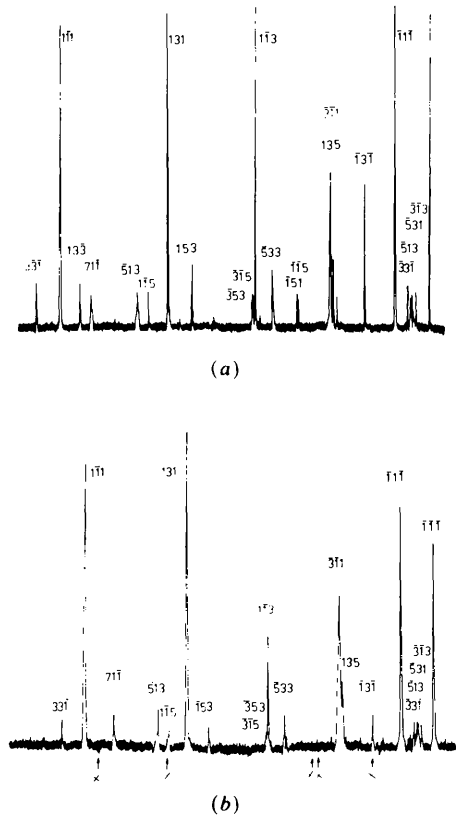

Fig. 4. (a) Multiple diffraction patterns of GaAs 222 Cu $K\alpha_1$ for (a) the unpolarized and (b) the σ-polarized beams. The 222 background is at 15% for (a) and 7% for (b) of the full scale of 4×10^3 counts s^{-1}.

Table 1. *Polarization factors B, π, P, FWHM η_T and the ratios (Exp, Th_B, Th_π, Th_p) of* Ge 111 *multiple diffractions*

	$\frac{2\bar{2}2}{1\bar{3}1}$	$\frac{\bar{2}\bar{4}2}{35\bar{1}}$	$\frac{\bar{1}33}{2\bar{2}\bar{2}}$	$\frac{2\bar{2}4}{1\bar{3}\bar{3}}$	$\frac{202}{11\bar{1}}$	$\frac{\bar{5}13}{60\bar{2}}$	$\frac{\bar{1}35}{2\bar{2}\bar{4}}$	$\frac{0\bar{2}6}{13\bar{5}}$	$\frac{3\bar{3}5}{44\bar{4}}$	$\frac{1\bar{1}1}{020}$	$\frac{\bar{4}00}{511}$	$\frac{\bar{2}42}{3\bar{3}\bar{1}}$
$B(\sigma+\pi)$	0·97	0·95	0·91	0·93	1·36	0·88	0·95	0·88	1·15	1·53	0·95	0·83
$B(\sigma)$	0·13	0·74	0·33	0·13	0·69	0·16	0·76	0·26	0·45	0·67	0·79	0·13
$\pi(\sigma+\pi)$	1·25	0·94	1·1	0·94	1·61	1·07	0·94	1·07	1·42	1·74	0·98	0·94
$\pi(\sigma)$	0·35	0·76	0·49	0·20	0·83	0·32	0·76	0·32	0·65	0·81	0·79	0·20
$P(\sigma+\pi)$	0·55	0·48	0·48	0·42	1·68	0·46	0·51	0·52	0·60	0·79	0·54	0·42
$P(\sigma)$	0·17	0·36	0·22	0·08	0·38	0·14	0·36	0·15	0·29	0·39	0·37	0·08
$(I_2-I_3)/I_2(\sigma+\pi)$	0·01	0·01	0·01	0·02	0·09	0·01	0·03	0·01	0·01	0·04	0·03	0·01
$(I_2-I_3)/I_2(\sigma)$	0	0·02	0	0	0·04	0	0·04	0	0	0	0·03	0
$\eta_T(\sigma+\pi)(0·01°)$	—	6	—		5	—	6				6	
$\eta_T(\sigma)(0·01°)$	—	13	—		10	—	12				11	
Exp	—	0·23			1·15		0·4				0·55	
Th_B		0·6			1		0·7				0·7	
Th_π		0·6			0·9		0·6				0·7	
Th_p		0·37			0·53		0·41				0·43	

of the term $p_{LM}(G)$ in (1) are listed in Table 1. More explicitly, B's and π's are defined as

$$B(\sigma)=\tfrac{1}{2}(B_0^2+B_3^2)/p_2 \tag{32}$$

$$B(\sigma+\pi)=a_2 \tag{33}$$

$$\pi(\sigma)=\pi_1 \tag{34}$$

$$\pi(\sigma+\pi)=\pi_1+\pi_6. \tag{35}$$

$P(\sigma)$ is the $p_{ij}(m)$ of (5) with $\alpha=44·72°$ and $P(\sigma+\pi)$ is the $p_{ij}(m)$ of (4). As can be seen, the $B(\sigma)$ of the σ-polarized-beam experiment is very small compared with the $B(\sigma+\pi)$ of the unpolarized-beam experiment, except for $\bar{2}\bar{4}2/35\bar{1}$, $202/11\bar{1}$, $\bar{1}35/2\bar{2}\bar{4}$, $\bar{4}00/511$ three-beam cases. The same is true for the π's and P's. The relative intensities for σ polarization of those three-beam diffractions with small $B(\sigma)$ values are too weak to be detected. Therefore, only the integrated-intensity ratios of strong diffractions which are experimentally observable are listed. Also in Table 1, the ratios of the measured integrated intensities over $\Delta\varphi$ between the unpolarized and σ-polarized beams, denoted as Exp, and the corresponding ratios Th_p, Th_π and Th_B calculated according to (1), (7) and (19), respectively, are also given. For comparison,

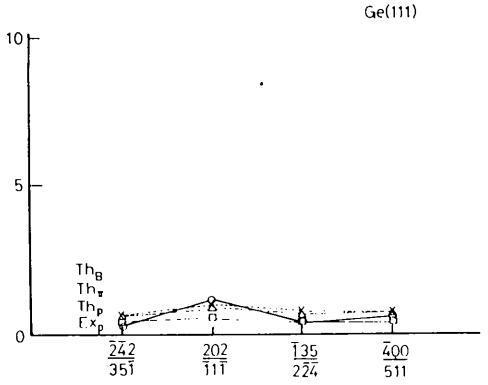

Fig. 5. Calculated Th_B, Th_π, Th_p and experimental Exp integrated-intensity ratios of Ge 111 multiple diffractions.

the calculated ratios and measured ratios are plotted in Fig. 5 for those strong three-beam diffractions. The experimental ratio of the strongest diffraction, $202/11\bar{1}$, deviates considerably from the calculated ratio, while those of relatively weak diffractions are in fair agreement with the calculated ones.

(ii) *Germanium* 222 *multiple diffractions*

Ge 222 is a space-group-forbidden reflection but with weak intensity due to covalent electrons. Hence, all the multiple diffractions with 222 as the primary reflection are of *Umweganregung* type ('peak'). As shown in Figs. 3(*a*) and (*b*), the intensities of the three-beam $3\bar{1}\bar{1}/\bar{1}33$, $\bar{1}\bar{1}3/33\bar{1}$, $5\bar{1}\bar{1}/\bar{3}33$, $1\bar{1}5/13\bar{3}$, $3\bar{1}5/\bar{1}33$ and $51\bar{1}/\bar{3}13$ decrease dramatically when the unpolarized incident beam is changed to σ polarized. These reflections are marked with arrows and ※ in Fig. 3(*b*). Table 2 lists the calculated polarization factors B's, π's and P's, measured peak intensities I_3/I_2, profile widths η_T and the integrated-intensity ratios, both experimental Exp and theoretical Th_B, Th_π and Th_p, for those reflections which are detectable in the σ-polarized-beam experiment. The intensity ratios are also plotted in Fig. 6. The curve denoted 'Exp' represents the measured $I_3(\sigma+\pi)/I_3(\sigma)$. Discrepancy occurs again for the strongest three-beam diffraction, *i.e.* $113/11\bar{1}$.

(iii) *Gallium arsenide* 222 *multiple diffractions*

GaAs 222 is not forbidden but is a very weak reflection. Most of the multiple diffractions are of *Umweg* type. Comparing Figs. 4(*a*) and (*b*), we find that, in the σ-polarized-beam experiment, $\bar{1}3\bar{1}/3\bar{1}3$ and $1\bar{1}3/13\bar{1}$ become weak reflections compared with the $\bar{1}1\bar{1}/313$ and $131/1\bar{1}1$ reflections, while the intensity of the four-beam $3\bar{1}1$, $135/531$, $1\bar{1}\bar{3}$ diffraction remains unchanged. In addition, the doublet $\bar{1}\bar{1}5/33\bar{3}$ and $\bar{1}51/3\bar{3}1$ almost disappears in Fig. 4(*b*). These are consistent with the small values of $B(\sigma)$, $\pi(\sigma)$ and $P(\sigma)$ given in Table 3. The measured peak-

Table 2. *Polarization factors B, π, P, FWHM η_T and the ratios (Exp, Th_B, Th_π, Th_p) of* Ge 222 *multiple diffractions*

	$\frac{3\bar{1}\bar{1}}{\bar{1}33}$	$\frac{1\bar{1}\bar{1}}{133}$	$\frac{3\bar{5}3}{\bar{1}7\bar{1}}$	$\frac{113}{11\bar{1}}$	$\frac{3\bar{5}1}{\bar{1}71}$	$\frac{3\bar{1}5}{\bar{1}3\bar{3}}$
$B(\sigma+\pi)$	0·57	0·97	1·16	1·14	0·97	0·55
$B(\sigma)$	0·29	0·84	0·66	0·64	0·73	0·34
$\pi(\sigma+\pi)$	0·88	1·2	1·45	1·44	1·2	0·65
$\pi(\sigma)$	0·35	0·85	0·82	0·8	0·85	0·4
$P(\sigma+\pi)$	0·29	0·48	0·57	0·57	0·48	0·29
$P(\sigma)$	0·09	0·15	0·28	0·29	0·14	0·03
$I_3/I_2(\sigma+\pi)$	6·44	16·62	2·15	26·33	2·02	2·77
$I_3/I_2(\sigma)$	1·27	2·58	1·35	2·82	1·28	1·24
$\eta_T(\sigma+\pi)(0·01°)$	4	4	10	4	11	4
$\eta_T(\sigma)(0·01°)$	9	11	14	11	13	16
Exp	2·24	2·3	1·14	3·35	1·36	0·55
Th_B	0·88	0·43	1·28	0·65	1·11	0·4
Th_π	1·1	0·5	1·28	0·65	1·2	0·4
Th_p	1·41	1·15	1·42	0·72	2·9	2·43

intensity ratios, $I_3/I_2(\sigma+\pi)$ and $I_3/I_2(\sigma)$, the measured integrated intensity ratios, $\mathrm{Ex}(t)=I_3(\sigma+\pi)/I_3(\sigma)$, and the calculated intensity ratios Th_B, Th_π and Th_p are also given in Table 3. Moreover, the large peak widths $\eta_T(\sigma+\pi)$, about 0·11°, for $\bar{5}33/7\bar{1}\bar{1}$ and $\bar{5}13/71\bar{1}$ are due to the large Lorentz factors, because these two reflections have small β_0 angles. [Note that the Lorentz factor is inversely proportional to $\sin\beta_0$ as indicated in (22*c*) and (22*d*).]

From (19)-(21), the relative intensity I'_G is the sum of I_D and I_K. For a centrosymmetric crystal like germanium, $I'_G(\Delta\varphi=0)=I_K(\Delta\varphi=0)$ according to (20) because $I_D(\Delta\varphi=0)=0$. What has been plotted in Fig. 6 is the kinematical intensities I_K for Ge. For the noncentrosymmetric GaAs, in order to plot I_K we ought to use (29) to determine the scale factor C_0. Following the same procedure previously reported (Tang & Chang, 1988) and plotting the ratios $I_{K,E}(\Delta\varphi=0)/I_K$ for all the three-beam reflections of the σ-polarized-beam experiment, we obtain the average scale factor equal to $C_0=6·37$ (see Fig. 7). Each point in Fig. 7 refers to a three-beam case. There

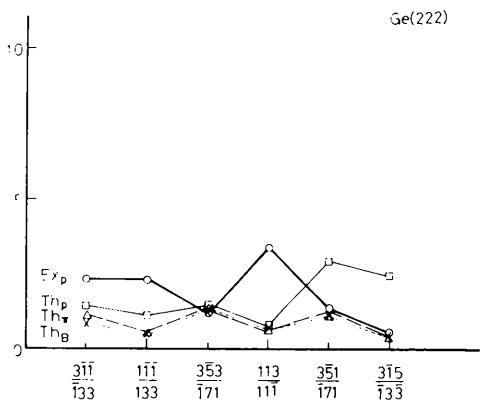

Fig. 6. Calculated Th_B, Th_π, Th_p and experimental Exp integrated-intensity ratios of Ge 222 multiple diffractions.

are 12 equivalent three-beam diffractions in each family $\{hkl\}$. The measured points are well distributed on both sides of the average C_0 line except for the case $\{\bar{1}31\}$. The scattered values of C in this case are probably due to the weak σ-polarized diffraction intensities (see Table 3 for the polarization factors) and the effect of crystal-surface inclination.

The purpose of using all 12 equivalent diffractions is to reduce the systematic errors caused by the surface inclination with respect to the (222) planes. These diffractions actually form six pairs, in which the two involved diffractions are separated in φ by 180°. The average intensity over these two diffractions should in principle not be affected by the surface inclination. The resultant errors in C, corrected by the crystal surface, are therefore smaller than the vertical bars indicated in Fig. 7. The errors, ΔC, are estimated to be about ±0·8 for $\{\bar{5}33\}$, ±0·5 for $\{\bar{1}\bar{1}3\}$ and ±0·3 for $\{1\bar{1}1\}$, $\{\bar{1}53\}$, $\{\bar{5}13\}$ and $\{\bar{1}\bar{1}1\}$. The overall error in C_0 is about ±0·4. This amounts to approximately 0·07 in $\Delta C_0/C_0$.

With this C_0 value, the experimental I_K's are determined. The kinematical ratios of peak intensities obtained experimentally, $\mathrm{Ex}(k)=I_K(\sigma+\pi)/I_K(\sigma)$, are plotted in Fig. 8, together with the integrated intensity ratios, $\mathrm{Ex}(t)=I_3(\sigma+\pi)/I_3(\sigma)$. Both Ex ($k$) and Ex ($t$) are listed in Table 3. The errors in Ex (k) and Ex (t) are about 10% of the measured values due to the errors in $\Delta C_0/C_0$ of the unpolarized (3%) (Chang & Tang, 1988) and the σ-polarized (7%) experiments. Clearly, the Ex (k) curve is in good agreement with the calculated curves Th_B, Th_π and Th_p, except for the weakest reflection, $1\bar{1}5/13\bar{3}$. This is probably attributable to the large error in intensity measurement. The curve Ex (t) resembles Ex (k) except for the two weak reflections $1\bar{1}5/13\bar{3}$ and $\bar{5}13/71\bar{1}$.

Incidentally, the triplet phases δ_3 associated with the three-beam diffractions of the σ-polarized-beam experiment are determined according to (30) and the procedure previously reported (Chang & Tang, 1988).

Table 3. *Polarization factors B, π, P, FWHM η_T and the ratios [Ex(t), Ex(k), Th_B, Th_π, Th_p] of* GaAs 222 *multiple diffractions*

	$\frac{1\bar{1}5}{13\bar{3}}$	$\frac{\bar{1}3\bar{1}}{3\bar{1}3}$	$\frac{\bar{1}\bar{1}1}{331}$	$\frac{1\bar{1}3}{13\bar{1}}$	$\frac{\bar{5}33}{7\bar{1}\bar{1}}$	$\frac{1\bar{1}1}{131}$	$\frac{\bar{5}13}{7\bar{1}\bar{1}}$
$B(\sigma+\pi)$	0·39	0·59	0·96	0·74	1·15	1·15	0·96
$B(\sigma)$	0·05	0·3	0·83	0·26	0·66	0·74	0·73
$\pi(\sigma+\pi)$	0·61	0·88	1·2	1·11	1·45	1·44	1·2
$\pi(\sigma)$	0·13	0·35	0·85	0·45	0·81	0·8	0·85
$P(\sigma+\pi)$	0·2	0·29	0·48	0·37	0·58	0·57	0·49
$P(\sigma)$	0·02	0·09	0·15	0·16	0·28	0·29	0·14
$I_3/I_2(\sigma+\pi)$	2·12	3·96	9·16	9·27	2·02	17·33	1·81
$I_3/I_2(\sigma)$	1·3	3·42	10·17	5·14	1·93	16·96	2·2
$\eta_T(\sigma+\pi)(0{\cdot}01°)$	7	8	8	7	11	8	12
$\eta_T(\sigma)(0{\cdot}01°)$	10	12	14	11	13	12	15
Ex(t)	1·12	0·79	0·51	1·15	0·85	0·66	0·64
Th_B	5·5	1·3	0·7	1·8	1·4	1·1	1
Th_π	3·3	1·6	0·8	1·6	1·5	1·2	1·1
Th_p	7	2·1	1·8	1·5	1·8	1·3	2·8
Ex(k)	2·17	0·79	0·68	1·15	0·77	0·79	1·04

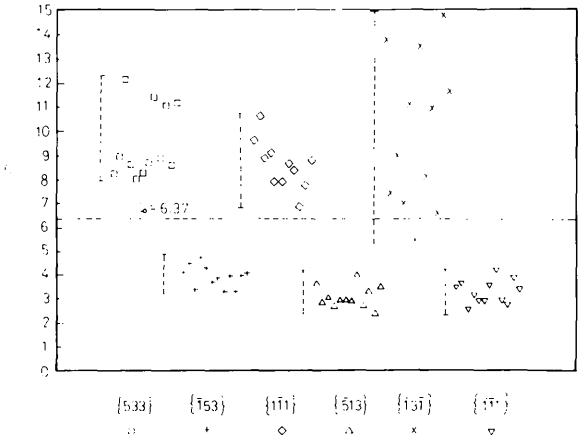

Fig. 7. Determination of the scale factor C_0 for GaAs 222 multiple diffractions of the σ-polarized-beam experiment. The vertical bars, indicating the scattering of the data points, are not the error bars (see text for details.)

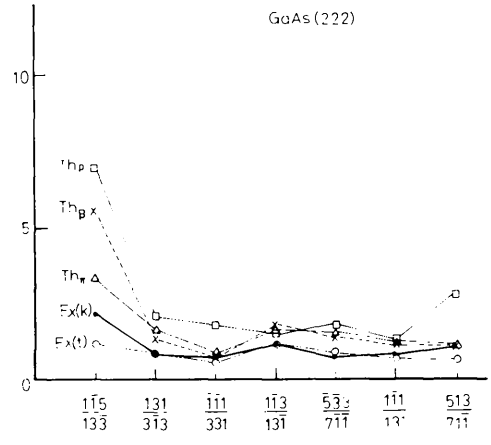

Fig. 8. Calculated (Th_B, Th_π, Th_p) and measured kinematical [Ex(k)] and total [Ex(t)] integrated-intensity ratios of GaAs 222 multiple diffractions. The errors in Ex(k) and Ex(t) are about 10% of the values indicated.

The determined phases are listed in Table 4 with relatively large errors, about ±20°, due to the weaker diffraction intensities and the error in C_0. The $\delta_E(\sigma+\pi)$ values are taken from Tang & Chang (1988).

V. Discussion and concluding remarks

In this paper the polarization factors a_2's, π's and p's are not strictly the conventional polarization factors but rather the ratios of the polarization factors for the three-beam and two-beam cases. Therefore, B's, π's and P's can be greater than unity.

The intensity ratios plotted in Figs. 5 and 6 for germanium show a disagreement between the calculated and the experimental results for very strong three-beam diffractions. This discrepancy is attributed to the fact that the kinematical theory is valid for weak reflections. It is therefore not surprising to see the invalidity of the kinematical approach for strong reflections. On the other hand, this disagreement does not occur for the GaAs 222 case. The strongest diffraction, $1\bar{1}1/131$, seems to have its intensity ratio close to the calculated one. This fact can be understood by comparing Tables 2 and 3 for Ge 222 and GaAs 222. By examining the terms $I_3/I_2(\sigma+\pi)$ and $I_3/I_2(\sigma)$, we find that the polarization plays a very important role in affecting the intensity ratios. For Ge 222, I_3/I_2 decreases drastically from 26·31 to 2·82 as the incident-beam polarization changes, while for GaAs 222 the change is merely from 17·33 to 16·96. This seems to explain the difference between the two cases. On the other hand, the intensity I_2 of Ge 222 is weaker than that of GaAs 222 and the phase of $1\bar{1}1/131$ of Ge is 90° different from that of GaAs. These facts could also affect the intensity ratios.

In Figs. 5, 6 and 8, the three theoretical curves almost have the same behavior. The intensity ratios Exp seem to be independent of the calculation model

Table 4. *Calculated triplet phases* (°) *of* GaAs 222 *for different polarized incident beams*; δ_T *is the exact triplet phase*

	$\bar{1}53$ / $3\bar{3}\bar{1}$	$\bar{1}3\bar{1}$ / $3\bar{1}3$	$\bar{1}\bar{1}1$ / $33\bar{1}$	$\bar{5}33$ / $7\bar{1}\bar{1}$	$1\bar{1}1$ / $13\bar{1}$	$\bar{5}13$ / $7\bar{1}\bar{1}$
δ_T	97	−72	97	−66	−74	98
$\delta_E(\sigma+\pi)$	98	−64	96	−69	−72	99
$\delta_E(\sigma)$	86	−65	82	−72	−76	102

chosen. Most surprisingly, the Th_π, not valid for calculating peak intensity (at $\Delta\varphi = 0$), gives reasonably good agreement with the experimental curves.

In conclusion, we have demonstrated experimentally how the beam polarizations affect multiple diffraction intensities and patterns. According to Juretschke (1986), the intensity asymmetry of a multiple diffraction profile may be reversed due to the influence of the dominant π-polarized waves under some special circumstances, for example the four-beam case, $1\bar{3}\bar{1}$ and 513 of Ge 222. In the present study, we have not encountered this situation for Ge and GaAs. It is, however, anticipated that with different crystals and wavelengths the predicted π-polarization effect could be encountered. Further experiments with well collimated synchrotron radiation are suggested for more precise measurement on multiply diffracted intensities of linearly polarized X-rays.

The authors are indebted to the National Science Council for financial support under contract no. NSC79-0208-M007-111. One of us (SWL) also thanks the same organization for providing a graduate fellowship during the course of this study.

Note added

Two papers (Alexandropoulos, McWhan, Juretschke & Kotsis, 1990; Schwegle, Hümmer & Weckert, 1990) on similar experiments with synchrotron radiation were reported at the 15th IUCr Congress, Bordeaux, France, 1990. The anomalous asymmetries of *N*-beam diffraction profiles have been encountered.

References

ALEXANDROPOULOS, N. G., MCWHAN, D., JURETSCHKE, H. J. & KOTSIS, K. (1990). *Acta Cryst.* A**46**, C416.

CATICHA-ELLIS, S. (1969). *Acta Cryst.* A**25**, 666-673.

CHANG, S. L. (1982). *Phys. Rev. Lett.* **48**, 163-166.

CHANG, S. L., HUANG, M. T., TANG, M. T. & LEE, C. H. (1989). *Acta Cryst.* A**45**, 870-878.

CHANG, S. L. & TANG, M. T. (1988). *Acta Cryst.* A**44**, 1065-1072.

CHAPMAN, L. D., YODER, D. R. & COLELLA, R. (1981). *Phys. Rev. Lett.* **46**, 1578-1581.

HØIER, R. & AANESTAD, A. (1981). *Acta Cryst.* A**37**, 787-794.

HÜMMER, K. & BILLY, H. W. (1982). *Acta Cryst.* A**38**, 841-848.

HÜMMER, K., WECKERT, E. & BONDZA, H. (1989). *Acta Cryst.* A**45**, 182-187.

JURETSCHKE, H. J. (1982*a*). *Phys. Rev. Lett.* **48**, 1487-1489.

JURETSCHKE, H. J. (1982*b*). *Phys. Lett.* **92A**, 183-185.

JURETSCHKE, H. J. (1986). *Phys. Status Solidi B*, **135**, 455-466.

LIPSCOMB, W. N. (1949). *Acta Cryst.* **2**, 193-194.

MO, F., HAUBACK, B. C. & THORKILDSEN, G. (1988). *Acta Chem. Scand. Ser. A*, **42**, 130-138.

MOON, R. M. & SHULL, C. G. (1964). *Acta Cryst.* **17**, 805-812.

POST, B. (1977). *Phys. Rev. Lett.* **39**, 760-763.

PRAGER, P. R. (1971). *Acta Cryst.* A**27**, 563-569.

RENNINGER, M. (1937). *Z. Phys.* **106**, 141-176.

SCHWEGLE, W., HÜMMER, K. & WECKERT, E. (1990). *Acta Cryst.* A**46**, C417.

SHEN, Q. & COLELLA, R. (1988). *Acta Cryst.* A**44**, 17-21.

TANG, M. T. & CHANG, S. L. (1988). *Acta Cryst.* A**44**, 1973-1078.

ZACHARIASEN, W. H. (1965). *Acta Cryst.* **18**, 705-710.

Acta Cryst. (1991). A**47**, 510-515

Electron Diffraction Structure Analysis of Diketopiperazine – a Direct Phase Determination

BY DOUGLAS L. DORSET

Electron Diffraction Department, Medical Foundation of Buffalo, Inc., 73 High Street, Buffalo, New York 14203, *USA*

(*Received* 2 *November* 1990; *accepted* 19 *March* 1991)

This paper is dedicated to Professor B. K. Vainshtein to celebrate his award of the Ewald Medal by the International Union of Crystallography

Abstract

Three-dimensional electron-diffraction intensity data from crystalline textures of diketopiperazine (2,5-piperazinedione) published by B. K. Vainshtein in 1955 [*Zh. Fiz. Kim.* (1955), **29**, 327-344] are found to be suitable for *ab initio* structure analysis *via* conventional direct phase determination based on the

0108-7673/91/050510-06$03.00